LETTER

Quantification of ocean heat uptake from changes in atmospheric O₂ and CO₂ composition

L. Resplandy[1]*, R. F. Keeling[2], Y. Eddebbar[2], M. K. Brooks[2], R. Wang[3], L. Bopp[4], M. C. Long[5], J. P. Dunne[6], W. Koeve[7] & A. Oschlies[7]

The ocean is the main source of thermal inertia in the climate system[1]. During recent decades, ocean heat uptake has been quantified by using hydrographic temperature measurements and data from the Argo float program, which expanded its coverage after 2007[2,3]. However, these estimates all use the same imperfect ocean dataset and share additional uncertainties resulting from sparse coverage, especially before 2007[4,5]. Here we provide an independent estimate by using measurements of atmospheric oxygen (O_2) and carbon dioxide (CO_2)—levels of which increase as the ocean warms and releases gases—as a whole-ocean thermometer. We show that the ocean gained $1.33 \pm 0.20 \times 10^{22}$ joules of heat per year between 1991 and 2016, equivalent to a planetary energy imbalance of 0.83 ± 0.11 watts per square metre of Earth's surface. We also find that the ocean-warming effect that led to the outgassing of O_2 and CO_2 can be isolated from the direct effects of anthropogenic emissions and CO_2 sinks. Our result—which relies on high-precision O_2 measurements dating back to 1991[6]—suggests that ocean warming is at the high end of previous estimates, with implications for policy-relevant measurements of the Earth response to climate change, such as climate sensitivity to greenhouse gases[7] and the thermal component of sea-level rise[8].

As shown in Fig. 1, recent temperature-based hydrographic estimates of ocean warming[9–12] show good agreement for the years 2007–2016 ($1.09 \pm 0.10 \times 10^{22}$ to $1.16 \pm 0.20 \times 10^{22}$ J yr^{-1}), but a larger spread when extending back to include the sparser data of the 1990s ($0.90 \pm 0.09 \times 10^{22}$ to $1.36 \pm 0.10 \times 10^{22}$ J yr^{-1} for 1993–2015). The spread is mostly caused by gap-filling methods and systematic errors[5,9], which together introduce uncertainties of up to 25%–50% in warming trends[4]. Because temperature-based estimates also use the same upper-ocean observations and linear warming trend for depths below 2,000 m (ref. [11]), they may share additional unknown systematic errors[12]. An alternative method based on the top of the atmosphere energy balance[13] is also not truly independent, because it is subject to large systematic errors when estimating long-term trends and therefore depends on the same hydrographic measurements for calibration[13–15]. Here we introduce a third method, based on changes in the abundances of gases in the atmosphere, which respond to whole-ocean warming through the temperature dependence of gas solubility in sea water. This method is not limited by data sparseness, because fast mixing in the atmosphere efficiently integrates the global ocean signal.

Changes in ocean heat content on seasonal[16] and glacial–interglacial[17] timescales have been reconstructed using measurements of noble gases in modern or ancient air. Our method is similar, but instead of relying on noble gases (for example, ratios of argon to nitrogen), which lack sufficient accuracy as yet[16], we rely on measurements of atmospheric O_2 and CO_2, which can be summed to yield a tracer 'atmospheric potential oxygen' (APO) that responds to warming similarly to a noble gas[18]. When the ocean warms, the solubility of O_2 and CO_2 drops, and the amount of gas lost by the ocean can be quantified with the complementary change observed in the atmosphere. Precise atmospheric

O_2 measurements began in 1991 (CO_2 in 1958), enabling APO-based reconstructions of ocean heat content that span nearly three decades[6].

APO ($O_2 + 1.1 \times CO_2$) is computed using observed atmospheric O_2/N_2 molar ratios and CO_2 molar fractions (see Methods)[6,19]. By design, APO is insensitive to exchanges with land ecosystems, which produce changes in O_2 and CO_2 that largely cancel in APO owing to their approximate 1.1 O_2/C oxidative ratio. Time-series measurements at remote sites show a global long-term decline in APO, with ΔAPO_{OBS} being -243.70 ± 10.10 per meg (units defined in the Methods) between 1991 and 2016. ΔAPO_{OBS} is driven by four primary contributors, illustrated in Fig. 2:

$$\Delta APO_{OBS} = \Delta APO_{FF} + \Delta APO_{Cant} + \Delta APO_{AtmD} + \Delta APO_{Climate} \quad (1)$$

where ΔAPO_{FF} is the decrease in APO caused by industrial processes (fossil-fuel burning and cement production), which in aggregate consume more than 1.1 moles of O_2 for each mole of CO_2 released; ΔAPO_{Cant} accounts for the oceanic uptake of excess anthropogenic atmospheric CO_2; ΔAPO_{AtmD} accounts for air–sea exchanges driven by ocean fertilization from anthropogenic aerosol deposition (increased fertilization leads to increased photosynthesis, with a concomitant release of O_2 and uptake of CO_2); and $\Delta APO_{Climate}$ accounts for air–sea fluxes of O_2, CO_2 and N_2 driven by ocean processes, including warming-induced changes in solubility, in ocean circulation, and in photosynthesis and respiration (N_2 influences O_2/N_2 ratios). Here, we derive $\Delta APO_{Climate}$ from equation (1) and show that it tracks ocean warming.

We estimate ΔAPO_{FF} using fossil-fuel and cement inventories[20], finding $\Delta APO_{FF} = -119.70 \pm 4.00$ per meg (Fig. 3). ΔAPO_{Cant} is controlled by the increase in atmospheric CO_2 and by ocean mixing, which is quantified by the distribution of transient tracers including chlorofluorocarbons (CFCs)[21]; we find that $\Delta APO_{Cant} = -154.30 \pm 4.20$ per meg. ΔAPO_{Cant} is relatively precise because it excludes the effects of changing ocean biology and circulation on natural carbon fluxes that are included in $\Delta APO_{Climate}$. ΔAPO_{AtmD} is derived from ocean model simulations with and without aerosol fertilization (phosphate, iron and nitrogen; Extended Data Fig. 1)[22]. ΔAPO_{AtmD} is uncertain, owing in part to uncertainties in iron availability to photosynthetic organisms, but is relatively small compared with the other terms: $\Delta APO_{AtmD} = 7.00 \pm 3.50$ per meg. From equation (1), we thereby find that $\Delta APO_{Climate} = 23.20 \pm 12.20$ per meg, corresponding to a least-squares linear trend of $+1.16 \pm 0.15$ per meg per year—larger than the trends expected from 26-year natural variations alone in four Earth-system models (the Community Earth System Model (CESM) and the Geophysical Fluid Dynamics Laboratory (GFDL), Institut Pierre Simon Laplace (IPSL) and University of Victoria (UVic) models). As shown in Fig. 3, a clear increase in $\Delta APO_{Climate}$ emerges over the period January 1991 to the end of December 2016.

A starting point for understanding $\Delta APO_{Climate}$ is to imagine that O_2 and CO_2 behave like inert gases, such that the air–sea fluxes are dominated by temperature-driven solubility changes. In this case,

[1]Department of Geosciences and Princeton Environmental Institute, Princeton University, Princeton, NJ, USA. [2]Scripps Institution of Oceanography, University of California San Diego, La Jolla, CA, USA. [3]Department of Environmental Science and Engineering, Fudan University, Shanghai, China. [4]LMD/IPSL, ENS, PSL Research University, École Polytechnique, Sorbonne Université, CNRS, Paris, France. [5]National Center for Atmospheric Research, Boulder, CO, USA. [6]NOAA, Geophysical Fluid Dynamics Laboratory, Princeton, NJ, USA. [7]GEOMAR Helmholtz Centre for Ocean Research Kiel, Kiel, Germany. *e-mail: laurer@princeton.edu
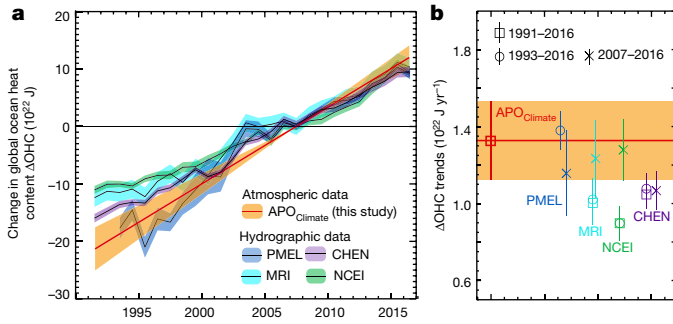
Fig. 1 | Change in global ocean heat content (ΔOHC). a, ΔOHC derived from hydrographic and atmospheric observations (normalized to zero in 2007, ±1σ uncertainty). **b**, Linear least-squares trends for 1991–2016, 1993–2016 and 2007–2016 (±1σ uncertainty). Hydrography-based ΔOHC estimates combine warming rates at ocean depths of 0 to 2,000 m (from Cheng and co-authors (CHEN)[12], Pacific Marine Environmental Laboratory (PMEL)[10], Meteorological Research Institute (MRI)[9] and National Centers for Environmental Information (NCEI)[31] estimates) with the revised deep ocean warming (at depths of more than 2,000 m) of ref. [11] (Extended Data Tables 1 and 2). The atmospheric-based estimate (this study), which uses observed atmospheric potential oxygen trends (ΔAPO$_{Climate}$) and model-based ΔAPO$_{Climate}$-to-ΔOHC ratios, does not resolve interannual variations.

APO would increase by around 0.8 per meg per 10^{22} J of warming, with changes in O_2 and CO_2 solubility accounting for an increase of +1.0 per meg per 10^{22} J, partly offset by the N_2 contribution of −0.2 per meg per 10^{22} J (Methods). Support for the dominance of solubility in ΔAPO$_{Climate}$ can be found in the natural distribution of O_2 and carbon in the ocean. Ocean potential oxygen (OPO) is a dissolved tracer that mirrors APO$_{Climate}$ and tracks changes in air–sea O_2 and CO_2 fluxes[18]. Observed OPO abundance is strongly tied to ocean potential temperature (Fig. 4): warming induces OPO loss, and cooling induces OPO gain. The observed OPO-to-temperature trend of −4.45 nmol J^{-1} is within 17% of the trend of −3.70 nmol J^{-1} expected from solubility alone (OPO$_{sat}$-to-temperature). Biological effects (related to changes in ocean circulation and photosynthesis/respiration) on CO_2 and O_2 substantially cancel in OPO (Extended Data Fig. 2), while thermal impacts reinforce each other, with warming waters releasing both O_2 and CO_2 to the atmosphere and increasing ΔAPO$_{Climate}$.

Further support for the dominance of solubility in ΔAPO$_{Climate}$ is found on multidecadal timescales in the four Earth-system models mentioned above, which yield OPO-to-temperature ratios of between −4.71 and −4.38 nmol J^{-1}, bracketing the ratio of −4.45 nmol J^{-1}

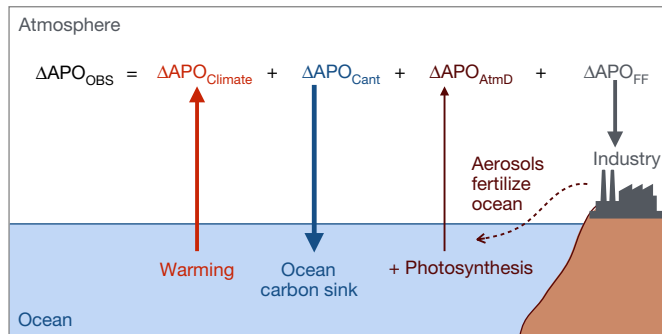**Fig. 2 | Processes contributing to observed changes in atmospheric potential oxygen (ΔAPO$_{OBS}$).** Industrial processes (fossil-fuel burning and cement production; ΔAPO$_{FF}$) and the ocean sink for anthropogenic carbon (ΔAPO$_{Cant}$) remove APO from the atmosphere. The fertilization effect of anthropogenic aerosol deposition (ΔAPO$_{AtmD}$)—which promotes marine photosynthesis—and the changes in solubility, biology and ocean circulation due to warming (ΔAPO$_{Climate}$) release APO into the atmosphere. Our study shows that ΔAPO$_{Climate}$ can be used to estimate long-term changes in global ocean warming.

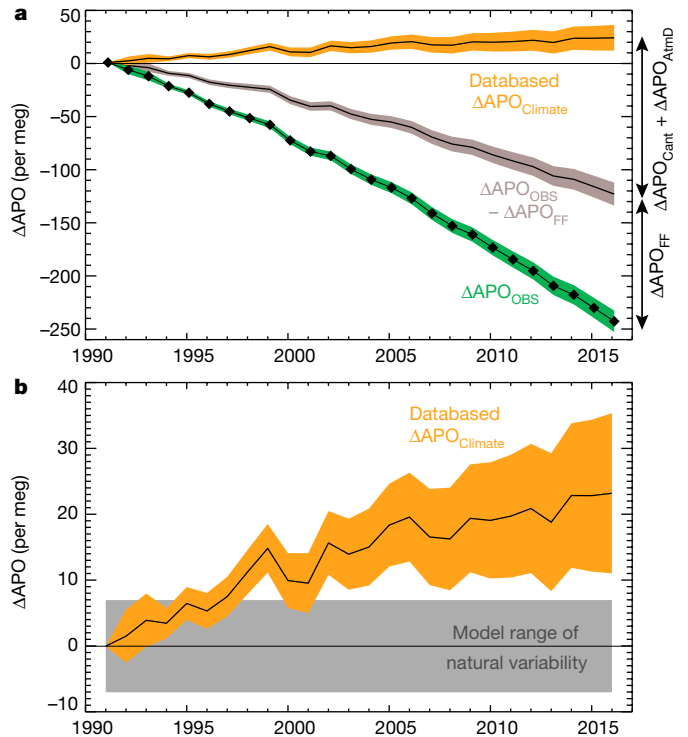**Fig. 3 | Databased estimates of global ΔAPO$_{Climate}$.**
a, ΔAPO$_{Climate}$ estimated from observed APO (ΔAPO$_{OBS}$) from the Scripps Institution of Oceanography network (1991–2016), and corrected by taking into account fossil-fuel burning, ocean anthropogenic carbon uptake and anthropogenic aerosol deposition (ΔAPO$_{Climate}$ = ΔAPO$_{OBS}$ − ΔAPO$_{FF}$ − ΔAPO$_{Cant}$ − ΔAPO$_{AtmD}$) and their 1σ uncertainty ranges. **b**, The increase in global ΔAPO$_{Climate}$ (±1σ interval) exceeds the range of 26-year trends expected from the natural variations in four Earth system models (CESM, GFDL, IPSL and UVic, shown in grey). Sources of uncertainty and contributions to ΔAPO$_{OBS}$, ΔAPO$_{FF}$ and ΔAPO$_{Cant}$ are given in Extended Data Tables 3 and 4.

found in hydrographic observations (Extended Data Fig. 3). The models also simulate a very close relationship between ΔAPO$_{Climate}$ and the change in global ocean heat content (ΔOHC) that occurs during the simulations (1920–2100), with an atmospheric build-up in APO of between 0.83 and 0.99 per meg per 10^{22} J (Extended Data Figs. 3, 4) —close to the ratio expected from temperature-driven solubility changes alone (0.8 per meg per 10^{22} J). By dividing the simulated APO change into separate biological and thermal components, we show that solubility changes account for more than 80% of ΔAPO$_{Climate}$, while biologically driven changes account for 5% to 20% (Extended Data Fig. 4). This partitioning found in response to transient warming is very similar to the partitioning found in hydrographic data (where solubility and biology contribute 83% and 17%, respectively, to the OPO-to-temperature ratio; Fig. 4).

Small differences between individual model ΔAPO$_{Climate}$-to-ΔOHC relationships (0.83 to 0.99 per meg per 10^{22} J) reflect systematic differences in biological fluxes. Models with stronger biological effects (IPSL and UVic) yield stronger oceanic loss of OPO and stronger release of APO for a given ocean warming (more negative OPO-to-temperature and higher ΔAPO$_{Climate}$-to-ΔOHC; Extended Data Fig. 3b). Using this relationship, we find that a ΔAPO$_{Climate}$-to-ΔOHC ratio of 0.87 ± 0.03 per meg per 10^{22} J is compatible with the observed OPO-to-temperature ratio. Combining this constrained ΔAPO$_{Climate}$-to-ΔOHC ratio (0.87 ± 0.03 per meg per 10^{22} J) with the observation-based trend in ΔAPO$_{Climate}$ (1.16 ± 0.18 per meg yr^{-1}) yields a warming trend of 1.33 ± 0.20 × 10^{22} J yr^{-1} between 1991 and 2016. As shown in Fig. 1, this APO-based estimate of ocean heat uptake agrees well, within uncertainties, with the highest temperature-based estimates (from the Pacific Marine Environmental Laboratory (PMEL)[10], available only for
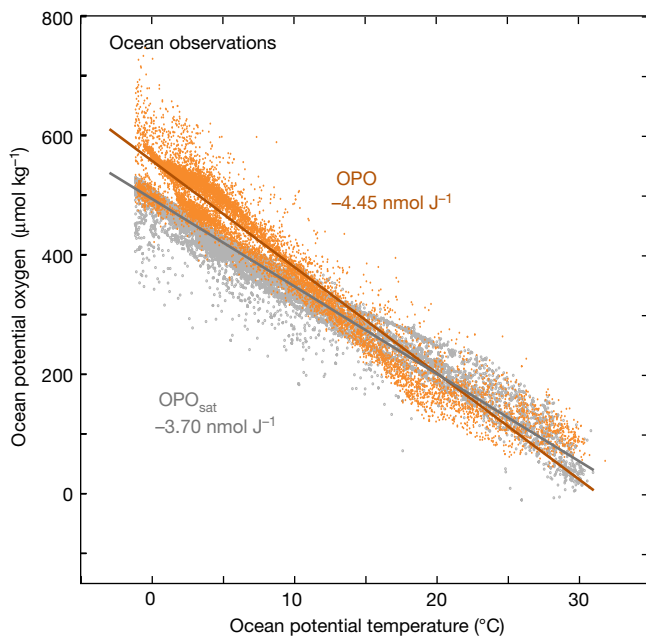
Fig. 4 | Observed link between potential oxygen and ocean heat. OPO concentrations in situ (OPO, yellow) and at saturation based on O_2 and CO_2 solubility (OPO$_{sat}$, grey) as a function of ocean temperature in the GLODAPv2 database[32].

1993–2015) and marginally with the two next estimates (from Cheng et al.[12] (CHEN) and the Japanese Meteorological Institute (MRI)[9]).

The APO data provide a much-needed independent confirmation of the recent upward revisions in estimates of ocean warming[5,9]. A higher value of ΔOHC compatible with both APO$_{Climate}$ and in situ temperature approaches (1.13 to 1.46×10^{22} J yr^{-1}) calls for a steric sea level rise of 1.34–1.74 mm yr^{-1} (Methods), in full agreement with satellite constraints on thermal expansion, corrected for the freshwater contribution (1.50 ± 0.40 mm yr^{-1})[8,23].

A higher ΔOHC will also affect the equilibrium climate sensitivity, recently estimated at between $+1.5$ K and $+4.5$ K if CO_2 is doubled[1]. This estimated range reflects a decrease in the lower bound from 2 K to 1.5 K owing to downward revision of the aerosol cooling effect (in the Intergovernmental Panel on Climate Change (IPCC) Fifth Assessment Report, as compared with the Fourth Assessment Report)[1,24], but relied on a low ΔOHC value (0.80×10^{22} J yr^{-1} for 1993–2010). An upward revision of the ocean heat gain by $+0.5 \times 10^{22}$ J yr^{-1} (to 1.30×10^{22} J yr^{-1} from 0.80×10^{22} J yr^{-1}) would push up the lower bound of the equilibrium climate sensitivity from 1.5 K back to 2.0 K (stronger warming expected for given emissions), thereby reducing maximum allowable cumulative CO_2 emissions by 25% to stay within the 2 °C global warming target (see Methods).

We find that the APO–heat coupling (APO$_{Climate}$) is most robust on decadal and longer timescales. Strong cancellation of biological O_2 and CO_2 fluxes is not expected on all temporal scales[25]. On seasonal timescales, air–sea O_2 fluxes driven by marine photosynthesis are around eight times larger than those of CO_2 owing to slow equilibration of CO_2 (ref. [25]). More complex coupling is also possible on interannual timescales[26], such as the weaker lagged air–sea CO_2 flux compared with the O_2 flux during El Niño events[27].

Atmospheric O_2 and CO_2 measurements have been applied previously to estimate global land and ocean CO_2 sinks, but relied on estimates of ocean heat content and model-based oceanic O_2-to-heat ratios to correct for climate-driven O_2 outgassing[28–30]. Here we have reversed this logic, using estimates of other quantities to constrain the ocean heating. Our approach exploits the APO–heat relationship, which is stronger than the O_2–heat relationship. Further work to constrain the separate contributions of O_2 and CO_2 to APO is needed to refine estimates of land and ocean carbon sinks using atmospheric O_2 and CO_2.

1. IPCC. *Climate Change 2013: The Physical Science Basis* (eds Stocker, T. F. et al.) (Cambridge Univ. Press, Cambridge, 2013).
2. Abraham, J. P. et al. A review of global ocean temperature observations: implications for ocean heat content estimates and climate change. *Rev. Geophys.* **51**, 450–483 (2013).
3. Riser, S. C. et al. Fifteen years of ocean observations with the global Argo array. *Nat. Clim. Change* **6**, 145–153 (2016).
4. Boyer, T. et al. Sensitivity of global upper-ocean heat content estimates to mapping methods, XBT bias corrections, and baseline climatologies. *J. Clim.* **29**, 4817–4842 (2016).
5. Cheng, L. et al. XBT science: assessment of instrumental biases and errors. *Bull. Am. Meteorol. Soc.* **97**, 924–933 (2016).
6. Keeling, R. F. & Manning, A. C. in *Treatise on Geochemistry* 385–404 (Elsevier, Oxford, 2014).
7. Forster, P. M. Inference of climate sensitivity from analysis of Earth's energy budget. *Annu. Rev. Earth Planet. Sci.* **44**, 85–106 (2016).
8. Church, J. A. et al. in *Climate Change 2013: The Physical Science Basis* (eds Stocker, T. F. et al.) 1137–1216 (IPCC, Cambridge Univ. Press, Cambridge, 2013).
9. Ishii, M. et al. Accuracy of global upper ocean heat content estimation expected from present observational data sets. *Sci. Online Lett. Atmos.* **13**, 163–167 (2017).
10. Johnson, G. C. et al. Ocean heat content. *Am. Meteorol. Soc. Bull.* **98**, S66–S68 (2017).
11. Desbruyères, D. G., Purkey, S. G., McDonagh, E. L., Johnson, G. C. & King, B. A. Deep and abyssal ocean warming from 35 years of repeat hydrography. *Geophys. Res. Lett.* **43**, 10356–10365 (2016).
12. Cheng, L. et al. Improved estimates of ocean heat content from 1960 to 2015. *Sci. Adv.* **3**, e1601545 (2017).
13. Allan, R. P. et al. Changes in global net radiative imbalance 1985–2012. *Geophys. Res. Lett.* **41**, 5588–5597 (2014).
14. Palmer, M. D. Reconciling estimates of ocean heating and Earth's radiation budget. *Curr. Clim. Change Rep.* **3**, 78–86 (2017).
15. Loeb, N. G. et al. Observed changes in top-of-the-atmosphere radiation and upper-ocean heating consistent within uncertainty. *Nat. Geosci.* **5**, 110–113 (2012).
16. Battle, M. *et al.* Measurements and models of the atmospheric Ar/N$_2$ ratio. *Geophys. Res. Lett.* **30**, 1786 (2003).
17. Ritz, S. P., Stocker, T. F. & Severinghaus, J. P. Noble gases as proxies of mean ocean temperature: sensitivity studies using a climate model of reduced complexity. *Quat. Sci. Rev.* **30**, 3728–3741 (2011).
18. Resplandy, L. et al. Constraints on oceanic meridional heat transport from combined measurements of oxygen and carbon. *Clim. Dyn.* **47**, 3335–3357 (2016); erratum **49**, 4317 (2017).
19. Stephens, B. B. et al. Testing global ocean carbon cycle models using measurements of atmospheric O_2 and CO_2 concentration. *Glob. Biogeochem. Cycles* **12**, 213–230 (1998).
20. Le Quéré, C. et al. Global carbon budget 2016. *Earth Syst. Sci. Data* **8**, 605–649 (2016).
21. DeVries, T. The oceanic anthropogenic CO_2 sink: storage, air-sea fluxes, and transports over the industrial era. *Glob. Biogeochem. Cycles* **28**, 631–647 (2014).
22. Wang, R. et al. Influence of anthropogenic aerosol deposition on the relationship between oceanic productivity and warming. *Geophys. Res. Lett.* **42**, 10745–10754 (2015).
23. Rietbroek, R., Brunnabend, S.-E., Kusche, J., Schröter, J. & Dahle, C. Revisiting the contemporary sea-level budget on global and regional scales. *Proc. Natl Acad. Sci. USA* **113**, 1504–1509 (2016).
24. IPCC. *Climate Change 2007: Synthesis Report* (eds Core Writing Team, Pachauri, R. K. & Reisinger, A.) (IPCC, Geneva, 2008).
25. Keeling, R. F. & Severinghaus, J. P. in *The Carbon Cycle* (eds Wigley, T. M. L. & Schimel, D.) 134–140 (Cambridge Univ. Press, New York, 2000).
26. Resplandy, L., Séférian, R. & Bopp, L. Natural variability of CO_2 and O_2 fluxes: what can we learn from centuries-long climate models simulations? *J. Geophys. Res. Oceans* **120**, 384–404 (2015).
27. Eddebbar, Y. A. et al. Impacts of ENSO on air-sea oxygen exchange: observations and mechanisms. *Glob. Biogeochem. Cycles* **31**, 2017GB005630 (2017).
28. Keeling, R. F. & Garcia, H. E. The change in oceanic O_2 inventory associated with recent global warming. *Proc. Natl Acad. Sci. USA* **99**, 7848–7853 (2002).
29. Bopp, L., Le Quéré, C., Heimann, M., Manning, A. C. & Monfray, P. Climate-induced oceanic oxygen fluxes: implications for the contemporary carbon budget. *Glob. Biogeochem. Cycles* **16**, 1022 (2002).
30. Keeling, C. D., Piper, S. C., Whorf, T. P. & Keeling, R. F. Evolution of natural and anthropogenic fluxes of atmospheric CO_2 from 1957 to 2003. *Tellus B Chem. Phys. Meteorol.* **63**, 1–22 (2011).

31. Levitus, S. et al. World ocean heat content and thermosteric sea level change (0–2000 m), 1955–2010. *Geophys. Res. Lett.* **39**, L10603 (2012).
32. Olsen, A. et al. The Global Ocean Data Analysis Project version 2 (GLODAPv2)—an internally consistent data product for the world ocean. *Earth Syst. Sci. Data* **8**, 297–323 (2016).

METHODS

Observed changes in APO. A change in atmospheric potential oxygen concentration (in per meg) is defined following[19]:

$$(\delta APO) = (\delta O_2/N_2) + \frac{1.1}{X_{O_2}} \times (X_{CO_2} - 350)$$

with

$$(\delta O_2/N_2) = \frac{O_2/N_2(\text{sample})}{O_2/N_2(\text{reference})} - 1$$

where $(\delta O_2/N_2)$ is the atmospheric change in $\delta O_2/N_2$ ratios (in per meg); X_{CO_2} is the CO_2 concentration in the air parcel (in p.p.m., that is, μmol mol^{-1}) and 350 is an arbitrary reference; 1.1 is the approximate O_2/CO_2 ratio of terrestrial ecosystems[33]; and X_{O_2} ($= 0.2094$) is the reference value of atmospheric mole fraction of O_2 necessary to convert X_{CO_2} from p.p.m. to per meg units.

ΔAPO_{OBS} is computed from in situ atmospheric changes in CO_2 concentrations and O_2/N_2 ratios[19] measured at stations of the Scripps Institution of Oceanography network (available online at http://scrippso2.ucsd.edu/)[6]. The global average ΔAPO_{OBS} is based on data from the three stations with longest record (1991 to 2016), that is, La Jolla (32.9° N, 117° W), Alert (82.5° N, 62.5° W) and Cape Grim (40.5° S, 144.5° E) and weighted by the stations' latitudinal distribution[34]. Station annual means are based on bimonthly data fit to a four-harmonic seasonal cycle and a stiff long-term trend[6]. The uncertainty on ΔAPO_{OBS} was computed by generating 10^6 time series with noise scaled to the random and systematic errors of APO data detailed in Extended Data Table 3. The uncertainty is taken as the 1σ interval (± 1 standard deviation) from these 10^6 realizations (Fig. 3).

Effects of fossil-fuel burning and cement production on APO. ΔAPO_{FF} is estimated using annual CO_2 emissions from oil, coal, gas, flaring and cement production ($\Delta CO_{2(i)}$ in moles)[20] weighted by their O_2/C combustion ratios, R_i (ref. [6]):

$$\Delta APO_{FF}(\text{per meg}) = \sum_i \frac{1.1 - R_i}{X_{O_2}} \times \frac{\Delta CO_{2(i)}}{M_{air}}$$

where M_{air} is the number of moles of dry air in the atmosphere (convert moles of CO_2 to p.p.m.).

The uncertainty on ΔAPO_{FF} includes uncertainties in CO_2 emissions ($\Delta CO_{2(i)}$)[35] and in combustion ratios (R_i in Extended Data Table 3)[36]. Uncertainties on $\Delta CO_{2(i)}$ are not independent in time and were estimated using an autoregressive model[37] (1,000 realizations); uncertainties on R_i were computed using a Monte Carlo approach (1,000 realizations). The uncertainty on ΔAPO_{FF} was then estimated by combining the 1,000 realizations of $\Delta CO_{2(i)}$ and the 1,000 realizations of R_i, yielding a set of 10^6 estimates of ΔAPO_{FF}.

Effect of ocean anthropogenic carbon uptake on APO. We represent the ocean CO_2 uptake (ΔCO_2) as the sum of three contributions:

$$\Delta CO_2 = \Delta Cant_0 + \Delta Cant' + \Delta CO_{2Climate} \quad (2)$$

where $\Delta Cant_0$ is the flux driven by the rise in CO_2 assuming steady ocean circulation ($\Delta Cant_0$ is negative, corresponding to uptake by the ocean); $\Delta CO_{2Climate}$ is the flux driven by the action of climate on natural carbon in the ocean ($\Delta CO_{2Climate}$ is positive, that is, warming reduces the uptake of natural carbon); and $\Delta Cant'$ is the remainder, which accounts for impact of circulation changes on the uptake of carbon driven by rising CO_2 ($\Delta Cant'$ is positive, that is, warming reduces the uptake of C_{ant}). ΔAPO_{Cant} can be expressed as the weighted sum of the two terms $\Delta Cant_0$ and $\Delta Cant'$:

$$\Delta APO_{Cant}(\text{per meg}) = \frac{1.1}{X_{O_2} \times M_{air}} \times (\Delta Cant_0 + \Delta Cant')$$

where $\Delta Cant_0$ and $\Delta Cant'$ are in moles. Note that $\Delta CO_{2Climate}$ is accounted for in $\Delta APO_{Climate}$.

$\Delta Cant_0$ is taken from a recent ocean inversion scheme with assimilation of observed potential temperature, salinity, radiocarbon and CFC-11 (ref. [21]), updated to 2016. $\Delta Cant'$ cannot be derived from observations and was estimated at 0.05 Pg C yr^{-1}, equivalent to a trend of $+0.2$ per meg^{-1}, using model simulations (see 'Model anthropogenic $\Delta Cant''$).

The uncertainty on ΔAPO_{Cant} is related to uncertainties in $\Delta Cant_0$ and $\Delta Cant'$. We allow for uncertainty in $\Delta Cant_0$ following ref. [21], using the ten sensitivity experiments (on ocean vertical and isopycnal diffusivities, data constraint, gas-exchange coefficient and so on) available for the ocean inversion and an estimate of the interannual variability in the ocean sink of a 0.2 Pg C yr^{-1}. We also allow an additional 1% uncertainty (less than 0.03 Pg C yr^{-1}) in $\Delta Cant_0$ resulting from imperfectly known atmospheric CO_2 history[38], taking account of sensitivity to start date (1765

versus 1791), to degree of temporal smoothing, and to using different versions of the record since 1958 (Mauna Loa record versus average of Mauna Loa and South Pole records). This estimate used a variant of the box-diffusion model[39], and CO_2 data from ref. [40] and the Scripps CO_2 program (https://library.ucsd.edu/dc/collection/bb3381541w). Uncertainties on $\Delta Cant'$ are assumed to be 100% of the model-based estimate of $\Delta Cant'$.

Ocean fertilization and atmospheric deposition of aerosols. Deposition of anthropogenic aerosol from fossil fuel, biomass burning and other processes fertilizes the ocean with nutrients and increases surface photosynthesis and subsurface respiration[41–43]. The effect of aerosol fertilization is partly counterbalanced by biological processes such as a decline in nitrogen fixation, which would be immediate, and an increase in denitrification in the water column, which would be on timescales of several hundred years[44]. Fixed anthropogenic nitrogen also fertilizes the land biosphere and coastal oceans by river runoffs, but, in these cases, efficient denitrification returns fixed nitrogen to the atmosphere and has little impact on the APO budget on the decadal timescales considered here. The impact of anthropogenic aerosol on O_2, CO_2 and APO air−sea fluxes is evaluated with the IPSL ocean model NEMO-PISCES v2 (ref. [45]), using the difference between simulations with aerosols and a simulation in which the aerosol deposition is fixed to a constant preindustrial value (equivalent to year 1850, Extended Data Fig. 1)[22]. We use four simulations with varying aerosols: one includes the combined effect of nitrogen (N), iron (Fe) and phosphorus (P) aerosol deposition, whereas the other three include only their individual contributions (N-only, Fe-only or P-only; Extended Data Fig. 1 and Extended Data Table 5). Uncertainties at the 1σ level on ΔAPO_{AtmD} are assumed to be $\pm 50\%$. See Extended Data Table 4.

Combined, N, Fe and P deposition accounts for an O_2 outgassing of 19.0 Tmol yr^{-1} for the 1980–2007 period (16 Tmol yr^{-1} for the entire 1960–2007 simulation period) and an oceanic CO_2 uptake of 8.3 Tmol yr^{-1} for the 1980–2007 period (6.8 Tmol yr^{-1} for the entire 1960–2007 simulation period; Extended Data Fig. 1 and Extended Data Table 5). The overall impact on ΔAPO_{AtmD} is $+0.27$ per meg yr^{-1} over 27 years of simulation (1980–2007), which we extrapolate to our 1991–2016 period. Increased O_2 outgassing accounts for an increase in APO of $+0.51$ per meg yr^{-1}, and CO_2 uptake accounts for a change in APO of -0.24 per meg yr^{-1} ($APO_{AtmD(O2)}$ and $APO_{AtmD(CO2)}$ in Extended Data Table 3).

The overall effect of N, Fe and P is smaller than the sum of the individual effects (Extended Data Fig. 1), because of the interplay between the aerosol deposition pattern and nutrient co-limitations in the ocean. Phytoplankton growth in the ocean depends on the availability of the most limiting nutrient. While more available N will promote photosynthesis in regions where N is limiting (for example, the tropical Atlantic Ocean), the effect is negligible in regions where Fe, P or any other nutrient is limiting (such as the Southern Ocean; see Fig. 2 in ref. [22]).

To our knowledge this is the first estimate of the effect of anthropogenic aerosol deposition on both O_2 and CO_2 air−sea fluxes at the global scale. Note however that ref. [6] used anthropogenic aerosol N inventories and scaling arguments to estimate an ocean O_2 loss due to anthropogenic N deposition only of about 10 ± 10 Tmol yr^{-1}, slightly lower than our model estimate of 15.5 Tmol yr^{-1}.

$\Delta APO_{Climate}$ trends and uncertainty analysis. We compute the APO response to climate change ($\Delta APO_{Climate}$) via:

$$\Delta APO_{Climate} = \Delta APO_{OBS} - \Delta APO_{FF} - \Delta APO_{Cant} - \Delta APO_{AtmD}$$

We combine the estimates of ΔAPO_{FF}, ΔAPO_{Cant} and ΔAPO_{AtmD} to obtain 10^6 time series of $\Delta APO_{FF} + \Delta APO_{Cant} + \Delta APO_{AtmD}$, and obtain 10^6 time series of $\Delta APO_{Climate}$ using the 10^6 time series of ΔAPO_{OBS}. We computed the $\Delta APO_{Climate}$ least-squares linear trend using the standard deviation of the 10^6 realizations of $\Delta APO_{Climate}$ as the error. We find a $\Delta APO_{Climate}$ trend of 1.16 ± 0.15 per meg yr^{-1} for 1991–2016.

Hydrography-based estimates of ocean heat uptake. We used four global-ocean estimates of ΔOHC, based on hydrographic measurements, in Fig. 1. Ocean warming rates from the surface to 2,000 m are from ref. [10] (PMEL), ref. [9] (MRI; https://climate.mri-jma.go.jp/pub/ocean/ts/v7.2/), an updated version of ref. [31] (NCEI; www.nodc.noaa.gov/OC5/3M_HEAT_CONTENT/basin_avt_data.html) and ref. [12] (CHEN; http://159.226.119.60/cheng/images_files/TOA_OHC_error-bar_1940_2015_2.txt), with the revised deep-ocean (depths greater than 2,000 m) constant linear warming rate of $0.10 \pm 0.03 \times 10^{22}$ J yr^{-1} of ref. [11] being based on the global ship-based sections program (GO-SHIP; http://www.go-ship.org)[46].

Ocean observations of ocean potential oxygen. We used in situ ocean observations from GLODAPv2 (ref. [32]) combined with an anthropogenic carbon estimate[21] interpolated at the location of each sample to compute 78,456 values (GLODAPv2 quality control $= 0$; marginal seas and coastal waters were removed) of OPO[18] as follows:

$$OPO = O_2^* + 1.1 \times C_{pi}^*$$

where O_2^* and C_{pi}^* are ocean conservative tracers related to air–sea fluxes of O_2 and preindustrial carbon[47]. The thermal component (solubility-driven) of OPO (OPO_{sat}) is computed as:

$$OPO_{sat} = O_{2sat} + 1.1 \times C_{pisat}$$

where O_{2sat} is the dissolved O_2 concentration at saturation with the observed temperature and salinity[48]; and C_{pisat} is the dissolved inorganic carbon concentration expected at the observed temperature and salinity and assuming equilibrium with a preindustrial partial pressure of CO_2 of 280 p.p.m., using pre-formed alkalinity[49].

Solubility-driven changes in OPO and APO. Extended Data Fig. 2 shows a tight and quasilinear link between observed OPO and potential temperature (-4.4 nmol J^{-1}; $r^2 = 0.95$), similar to the link found between OPO_{sat} and potential temperature (-3.7 nmol J^{-1}; $r^2 = 0.93$). This suggests that changes in OPO and hence $\Delta APO_{Climate}$ are driven primarily by changes in thermal air–sea fluxes. In these observations, departures of dissolved oxygen and carbon concentrations (O_2^* and C_{pi}^*) from their respective saturation curves (O_{2sat} and C_{pisat}) due to biological activity tend to balance (Extended Data Fig. 2). By contrast, thermal effects reinforce each other (O_{2sat} and C_{pisat} both decrease with increasing temperature) and biological effects compensate for each other ($O_2^* > O_{2sat}$ and $C_{pi}^* < C_{pisat}$).

The change in APO expected from changes in gas solubility in the ocean is an increase of 3.0 nmol per J of warming, which includes the outgassing of O_2 and CO_2 following OPO_{sat} (3.7 nmol J^{-1}) and the release of N_2 (0.7 nmol J^{-1}) (Extended Data Fig. 2b). A change of 3.0 nmol per J of warming is equivalent to an increase of 1.0 per meg per 10^{22} J ($= (3.0 \times 10^{-9}) / (3.7 \times 10^{19}) \times 10^{22} = 0.8 \times 10^{-6} = 1.0$ per meg per 10^{22} J, with 3.7×10^{19} being the number of moles of O_2 in the atmosphere). O_2 and CO_2 solubility alone yields an increase in APO of 1.0 per meg per 10^{22} J, which is partly counterbalanced by the outgassing of N_2 that decreases APO by 0.2 per meg per 10^{22} J (via the increase in the O_2/N_2 ratio).

Earth system model experiments. We used four Earth-system models (ESMs): the Geophysical Fluid Dynamics Laboratory Earth System Models with a nominally level vertical coordinate version, GFDL-ESM2M (called GFDL here)[50,51], the Institut Pierre-Simon Laplace Coupled Model 5 version IPSL-CM5A-LR (IPSL here)[52], the Community Earth System Model large ensemble CESM-LE (CESM here)[53] and the UVic model version 2.9 (UVic here)[54]. Evaluation of these models and their biogeochemical components can be found in previous studies[51,55–57]. GFDL, IPSL and UVic participated in the Coupled Model Intercomparison Project Phase 5 (CMIP5)[58].

For GFDL, IPSL and UVic, we used the CMIP5 business as usual 'historical-RCP8.5' scenario, the feedback experiment 'esmFdbk3' (which includes only warming-driven changes associated with anthropogenic emissions, such as radiation effects), and the fixed-climate experiment 'esmFixClim3', which includes only the direct biogeochemical effects of increasing atmospheric CO_2 (for example, uptake of anthropogenic carbon, acidification and so on). For CESM, we also used the historical-RCP8.5 experiment and the separation between anthropogenic carbon from the natural carbon available in this model (carbon tracer separation approach). The feedback approach used for GFDL, IPSL and UVic removes all direct biogeochemical effects of rising atmospheric CO_2 on the air–sea O_2 and CO_2 exchanges, whereas the natural carbon tracer separation approach used for CESM still includes the biogeochemical impacts of increasing atmospheric CO_2 on the carbon cycle (for example, acidification) even while it excludes the anthropogenic carbon itself. However, we expect the effect on our results to be small and negligible.

We also used the multicentury preindustrial control simulation 'piControl' with no increase in atmospheric CO_2 to correct for model drift and to estimate the natural internal variability of $\Delta APO_{Climate}$ (Fig. 2). We used model results over the 1920–2100 period, which were available for the four models.

Model OPO was computed as for the observations. Note that for CESM we removed subsurface regions of high denitrification in the Eastern Equatorial Pacific Ocean and the Bay of Bengal, where oxygen and O_2^* in this model have unrealistic values[59].

Model anthropogenic $\Delta Cant'$. The component $\Delta Cant'$ was derived from equation (2) ($\Delta Cant' = \Delta CO_2 - \Delta Cant_0 - \Delta CO_{2Climate}$) using CMIP5 model simulations. ΔCO_2 was taken from experiment RCP8.5, $\Delta Cant_0$ from experiment esmFixClim3, and $\Delta CO_{2Climate}$ from experiment esmFdbk3. Note that the control simulation was also used to correct model drift. We estimated $\Delta Cant'$ to be 0.05 ± 0.05 Pg C yr^{-1} for 1991–2016, based on the results of the three models—which individually yielded $\Delta Cant'$ values of 0.0 Pg C yr^{-1} (IPSL), 0.12 Pg C yr^{-1} (GFDL) and 0.12 Pg C yr^{-1} (UVic)—and assuming an uncertainty of $\pm 100\%$. This corresponds to a trend of 0.12 ± 0.12 per meg yr^{-1}.

Model $\Delta APO_{Climate}$-to-ΔOHC ratios and uncertainty. Model $\Delta APO_{Climate}$ is computed using individual contributions from O_2, CO_2 and N_2 as follows:

$$APO_{Climate}(\text{per meg}) = APO_{O_2} + APO_{CO_2} + APO_{N_2}$$

$$\Delta APO_{Climate}(\text{per meg}) = \frac{1}{X_{O_2} 2p M_{air}}$$
$$\times \left(\Delta F_{O_2} + 1.1 \times \Delta F_{CO_2} - \frac{X_{O_2}}{X_{N_2}} \times \Delta F_{N_2} \right)$$

where ΔF_{O_2}, ΔF_{CO_2} and ΔF_{N_2} are the changes in air–sea fluxes of O_2, CO_2 and N_2 respectively (in moles); M_{air} is the number of moles of dry air in the atmosphere; and X_{N_2}, X_{O_2} are the reference atmospheric mixing ratios of N_2 and O_2 respectively[60]. O_2 and CO_2 fluxes are simulated in the models. N_2 air–sea fluxes, which affect the O_2 atmospheric mixing ratio (because O_2 constitutes around 20% of the atmospheric composition), are quantified from the global ocean temporal changes in N_2 solubility computed from model changes in temperature and salinity[61].

The link between long-term changes in $APO_{Climate}$ and ocean heat content—that is, $\Delta APO_{Climate}$-to-ΔOHC ratios—were computed for each model using the 180 years of simulations (1920–2100). Resulting $\Delta APO_{Climate}$-to-ΔOHC ratios vary between 0.83 and 0.99 per meg per 10^{22} J of warming (Extended Data Fig. 3). These ratios include uncertainty in the natural climate variations on interannual and decadal timescales and uncertainty in the O_2/C oxidative ratio associated with global gains and losses of O_2 and CO_2 by terrestrial ecosystems. The uncertainty due to interannual variations was evaluated by computing $\Delta APO_{Climate}$-to-ΔOHC ratios using multiple 26-year-long segments from the 180-year simulations. We obtained 616 $\Delta APO_{Climate}$-to-ΔOHC ratios (154 time series of 26 years per model), and used the standard deviation between these ratios as a measure of the uncertainty.

The O_2/C ratio is assumed to be 1.1 in our computation to follow the widely accepted definition of APO (APO = $O_2 + 1.1 \times CO_2$), but is shown to have variations between 1 and 1.1 (ref. [33]). An oxidative ratio lower than 1.1 would yield a weaker $\Delta APO_{Climate}$-to-ΔOHC slope and hence a slightly higher estimate of ΔOHC for a given $\Delta APO_{Climate}$. We evaluated the influence of the O_2/C ratio for each model by using the difference between $\Delta APO_{Climate}$ computed with a ratio of 1.1 and $\Delta APO_{Climate}$ computed with a ratio of 1. The two contributions to the uncertainties on the simulated $\Delta APO_{Climate}$-to-ΔOHC ratios (interannual variations and O_2/C ratio) combine to yield ± 0.01 per meg per 10^{22} J for the CESM and GFDL models, ± 0.02 per meg per 10^{22} J for the UVic model, and ± 0.05 per meg per 10^{22} J for the IPSL model (1σ). These uncertainties are used in Extended Data Fig. 3.

Steric component of sea-level rise. We evaluated the steric component of sea-level rise associated with a ΔOHC compatible with both $APO_{Climate}$ and existing in situ temperature constraints (that is, between 1.13×10^{22} J yr^{-1} and 1.46×10^{22} J yr^{-1}) to be between 1.34 mm yr^{-1} and 1.74 mm yr^{-1}. Following ref. [62], this calculation assumes that 45% of the warming occurs below 700 m, and that the steric rise is 1 mm per 0.60×10^{22} J above 700 m, and 1 mm per 1.15×10^{22} J below 700 m (that is, a global steric rise of 1 mm per 0.84×10^{22} J). Assuming that 48% of the warming occurs below 700 m (ref. [10]) would yield a global steric rise of 1 mm per 0.86×10^{22} J and change our estimate by less than 3%. Our estimate is also consistent with the recent hydrography-based estimate of the WCRP Global Sea Level Budget Group[63].

Ocean heat uptake, sea level and climate sensitivity. Climate sensitivity has been estimated to fall within the range of $+1.5$ K to $+4.5$ K for a doubling of CO_2 (ref. [1]). The impact of an increase in the ocean heat uptake on the effective equilibrium climate sensitivity (the apparent equilibrium climate sensitivity diagnosed from nonequilibrium conditions) can be estimated using a cumulative approach on the Earth energy balance (see Fig. 2 in ref. [1]):

$$N = F - \alpha \Delta T \tag{3}$$

where N is the global heat imbalance, which mostly consists of the ocean heat uptake; F is the radiative forcing (in W m^{-2}); ΔT is the increase in surface temperature (in K) above a natural steady state; and α is the climate feedback parameter (in W m^{-2} K^{-1}), which is inversely proportional to the effective equilibrium climate sensitivity[1]. All terms in equation (3) are time integrated over the period of interest. The IPCC Fifth Assessment Report gives a ΔOHC of 0.80×10^{22} J yr^{-1} for 1993–2010, which is about 0.5×10^{22} J yr^{-1} lower than the ΔOHC that is compatible with both APO and hydrographic constraints. By applying equation (3)[1] to surface temperature data over the period 1991–2016 (HadCrut4 version 4.5, ref. [64], with a 1860–1879 preindustrial baseline), we found that the upward revision of the global heat imbalance, N, by $+0.5 \times 10^{22}$ J yr^{-1} pushes up the lower bound of the equilibrium climate sensitivity from 1.5 K back to 2.0 K. An increase of the lower bound from 1.5 K to 2 K corresponds to a need to reduce maximum emissions by 25% to stay within the 2 °C global warming target (because of the almost linear

relationship between warming and cumulative emissions; see Fig. SPM.10 in ref. [1]). This corresponds to a reduction in maximum allowable cumulative CO_2 emissions from 4,760 Gt CO_2 to 3,570 Gt CO_2.

We tested the sensitivity of the climate sensitivity by using three alternate temperature datasets (NASA GISS Surface Temperature Analysis GISTEMP[65], available at https://data.giss.nasa.gov/gistemp; the NOAA/OAR/ESRL global surface temperature data[66] v4.0.1, available at https://www.esrl.noaa.gov/psd; and the ocean + land product of Berkeley Earth, available at berkeleyearth.lbl.gov/auto/Global; all data were accessed on 7 August 2018) as well as two preindustrial baseline periods (1860–1879 and 1880–1899). We find changes in the climate sensitivity of the order of 5% owing to the choice of temperature dataset, and less than 1% due to the choice of preindustrial baseline.

Link to global ocean deoxygenation. Our application of O_2 atmospheric measurements to constrain long-term ocean warming can be compared with earlier work that considers warming-driven oceanic O_2 outgassing. Multiplying our warming rate of $1.33 \pm 0.20 \times 10^{22}$ J yr^{-1} by the O_2-to-heat ratios simulated by the four ESMs (-3.70 ± 0.80 nmol O_2 J^{-1}) yields an ocean loss of 49 ± 13 Tmol O_2 yr^{-1}. Adding a loss of around 19 ± 19 Tmol O_2 yr^{-1} due to anthropogenic aerosols (Extended Data Table 5) yields a global ocean outgassing of 68 ± 23 Tmol O_2 yr^{-1}, in the range of previous estimates based on atmospheric data[67] (about 40 Tmol O_2 yr^{-1}), ocean data above 1,000 m (55–65 Tmol O_2 yr^{-1}, refs [68,69]) and global ocean data[70] (96 ± 42 Tmol O_2 yr^{-1}). This calculation suggests that ocean CO_2 uptake is reduced by warming at a ratio of around 0.70 nmol of CO_2 per joule (the difference between the O_2-to-heat ratio of 3.70 nmol J^{-1} and the OPO-to-heat ratio of 4.45 nmol J^{-1}).

Code availability. ESM codes are available online for IPSL-CM5A-LR (cmc.ipsl.fr/ipsl-climate-models), GFDL-ESM2M (mdl-mom5.herokuapp.com/web/docs/project/quickstart), UVic (climate.uvic.ca/model) and CESM (www.cesm.ucar.edu/models/).

Data availability

Scripps APO data are available at http://scrippso2.ucsd.edu/apo-data. APO$_{Climate}$ data, contributions to APO$_{OBS}$ and ocean heat content time series are available in Extended Data Figs. 1–4 and Extended Data Tables 1–5. Model results are available upon reasonable request to R.W. (IPSL anthropogenic aerosol simulations), L.B. (IPSL-CM5A-LR), M.C.L. (CESM-LE), J.P.D. (GFDL-ESM2M) or W.K. (UVic).

33. Severinghaus, J. P. *Studies of the Terrestrial O2 and Carbon Cycles in Sand Dune Gases and in Biosphere*. PhD Thesis, Columbia Univ. (1995).
34. Hamme, R. C. & Keeling, R. F. Ocean ventilation as a driver of interannual variability in atmospheric potential oxygen. *Tellus B Chem. Phys. Meteorol.* **60**, 706–717 (2008).
35. Andres, R. J., Boden, T. A. & Higdon, D. A new evaluation of the uncertainty associated with CDIAC estimates of fossil fuel carbon dioxide emission. *Tellus B Chem. Phys. Meteorol.* **66**, 23616 (2014).
36. Keeling, R. F., Manning, A. C., Paplawsky, W. J. & Cox, A. C. On the long-term stability of reference gases for atmospheric O2/N2 and CO2 measurements. *Tellus B Chem. Phys. Meteorol.* **59**, 3–14 (2007).
37. Ballantyne, A. P. et al. Audit of the global carbon budget: estimate errors and their impact on uptake uncertainty. *Biogeosciences* **12**, 2565–2584 (2015).
38. Bronselaer, B., Winton, M., Russell, J., Sabine, C. L. & Khatiwala, S. Agreement of CMIP5 simulated and observed ocean anthropogenic CO2 uptake. *Geophys. Res. Lett.* **44**, 12298–12305 (2017).
39. Oeschger, H., Siegenthaler, U., Schotterer, U. & Gugelmann, A. A box diffusion model to study the carbon dioxide exchange in nature. *Tellus* **27**, 168–192 (1975).
40. MacFarling Meure, C. et al. Law Dome CO2, CH4 and N2O ice core records extended to 2000 years BP. *Geophys. Res. Lett.* **33**, L14810 (2006).
41. Wang, D., Gouhier, T. C., Menge, B. A. & Ganguly, A. R. Intensification and spatial homogenization of coastal upwelling under climate change. *Nature* **518**, 390–394 (2015).
42. Ito, T., Nenes, A., Johnson, M. S., Meskhidze, N. & Deutsch, C. Acceleration of oxygen decline in the tropical Pacific over the past decades by aerosol pollutants. *Nat. Geosci.* **9**, 443–447 (2016).
43. Jickells, T. D. et al. A reevaluation of the magnitude and impacts of anthropogenic atmospheric nitrogen inputs on the ocean. *Glob. Biogeochem. Cycles* **31**, 289–305 (2017).
44. Somes, C. J., Landolfi, A., Koeve, W. & Oschlies, A. Limited impact of atmospheric nitrogen deposition on marine productivity due to biogeochemical feedbacks in a global ocean model. *Geophys. Res. Lett.* **43**, 4500–4509 (2016).
45. Aumont, O., Ethé, C., Tagliabue, A., Bopp, L. & Gehlen, M. PISCES-v2: an ocean biogeochemical model for carbon and ecosystem studies. *Geosci. Model Dev.* **8**, 2465–2513 (2015).
46. Talley, L. D. et al. Changes in ocean heat, carbon content, and ventilation: a review of the first decade of GO-SHIP global repeat hydrography. *Annu. Rev. Marine Sci.* **8**, 185–215 (2016).
47. Sarmiento, J. L. & Gruber, N. Sinks for anthropogenic carbon. *Phys. Today* **55**, 30–36 (2002).
48. Garcia, H. E. & Gordon, L. I. Oxygen solubility in seawater: better fitting equations. *Limnol. Oceanogr.* **37**, 1307–1312 (1992).
49. Gruber, N., Sarmiento, J. L. & Stocker, T. F. An improved method for detecting anthropogenic CO2 in the oceans. *Glob. Biogeochem. Cycles* **10**, 809–837 (1996).
50. Dunne, J. P. et al. GFDL's ESM2 global coupled climate–carbon Earth system models. Part I: physical formulation and baseline simulation characteristics. *J. Clim.* **25**, 6646–6665 (2012).
51. Dunne, J. P. et al. GFDL's ESM2 global coupled climate–carbon Earth system models. Part II: carbon system formulation and baseline simulation characteristics. *J. Clim.* **26**, 2247–2267 (2013).
52. Séférian, R., Iudicone, D., Bopp, L., Roy, T. & Madec, G. Water mass analysis of effect of climate change on air–sea CO2 fluxes: the Southern Ocean. *J. Clim.* **25**, 3894–3908 (2012).
53. Kay, J. E. et al. The Community Earth System Model (CESM) large ensemble project: a community resource for studying climate change in the presence of internal climate variability. *Bull. Am. Meteorol. Soc.* **96**, 1333–1349 (2015).
54. Keller, D. P., Oschlies, A. & Eby, M. A new marine ecosystem model for the University of Victoria Earth System Climate Model. *Geosci. Model Dev.* **5**, 1195–1220 (2012).
55. Bopp, L. et al. Multiple stressors of ocean ecosystems in the 21st century: projections with CMIP5 models. *Biogeosciences* **10**, 6225–6245 (2013).
56. Keller, D. P., Kriest, I., Koeve, W. & Oschlies, A. Southern Ocean biological impacts on global ocean oxygen. *Geophys. Res. Lett.* **43**, 6469–6477 (2016).
57. Long, M. C., Deutsch, C. & Ito, T. Finding forced trends in oceanic oxygen. *Glob. Biogeochem. Cycles* **30**, 381–397 (2016).
58. Taylor, K. E., Stouffer, R. J. & Meehl, G. A. An overview of CMIP5 and the experiment design. *Bull. Am. Meteorol. Soc.* **93**, 485–498 (2012).
59. Moore, J. K., Lindsay, K., Doney, S. C., Long, M. C. & Misumi, K. Marine ecosystem dynamics and biogeochemical cycling in the Community Earth System Model [CESM1(BGC)]: comparison of the 1990s with the 2090s under the RCP4.5 and RCP8.5 scenarios. *J. Clim.* **26**, 9291–9312 (2013).
60. Rödenbeck, C., Le Quéré, C., Heimann, M. & Keeling, R. F. Interannual variability in oceanic biogeochemical processes inferred by inversion of atmospheric O2/N2 and CO2 data. *Tellus B Chem. Phys. Meteorol.* **60**, 685–705 (2008).
61. Hamme, R. C. Mechanisms controlling the global oceanic distribution of the inert gases argon, nitrogen and neon. *Geophys. Res. Lett.* **29**, 35-1–35-4 (2002).
62. Trenberth, K. E., Fasullo, J. T., von Schuckmann, K. & Cheng, L. Insights into Earth's energy imbalance from multiple sources. *J. Clim.* **29**, 7495–7505 (2016).
63. WCRP Global Sea Level Budget Group. Global sea level budget 1993–present. *Earth Syst. Sci. Data* **10**, 1551–1590 (2018).
64. Morice, C. P., Kennedy, J. J., Rayner, N. A. & Jones, P. D. Quantifying uncertainties in global and regional temperature change using an ensemble of observational estimates: the HadCRUT4 data set. *J. Geophys. Res. Atmos.* **117**, D08101 (2012).
65. Hansen, J., Ruedy, R., Sato, M. & Lo, K. Global surface temperature change. *Rev. Geophys.* **48**, RG4004 (2010).
66. Vose, R. S. et al. NOAA's merged land–ocean surface temperature analysis. *Bull. Am. Meteorol. Soc.* **93**, 1677–1685 (2012).
67. Keeling, R. F., Körtzinger, A. & Gruber, N. Ocean deoxygenation in a warming world. *Annu. Rev. Mar. Sci.* **2**, 199–229 (2010).
70. Schmidtko, S., Stramma, L. & Visbeck, M. Decline in global oceanic oxygen content during the past five decades. *Nature* **542**, 335–339 (2017).
68. Helm, K. P., Bindoff, N. L. & Church, J. A. Observed decreases in oxygen content of the global ocean. *Geophys. Res. Lett.* **38**, L23602 (2011).
69. Ito, T., Minobe, S., Long, M. C. & Deutsch, C. Upper ocean O2 trends: 1958–2015. *Geophys. Res. Lett.* **44**, 4214–4223 (2017).
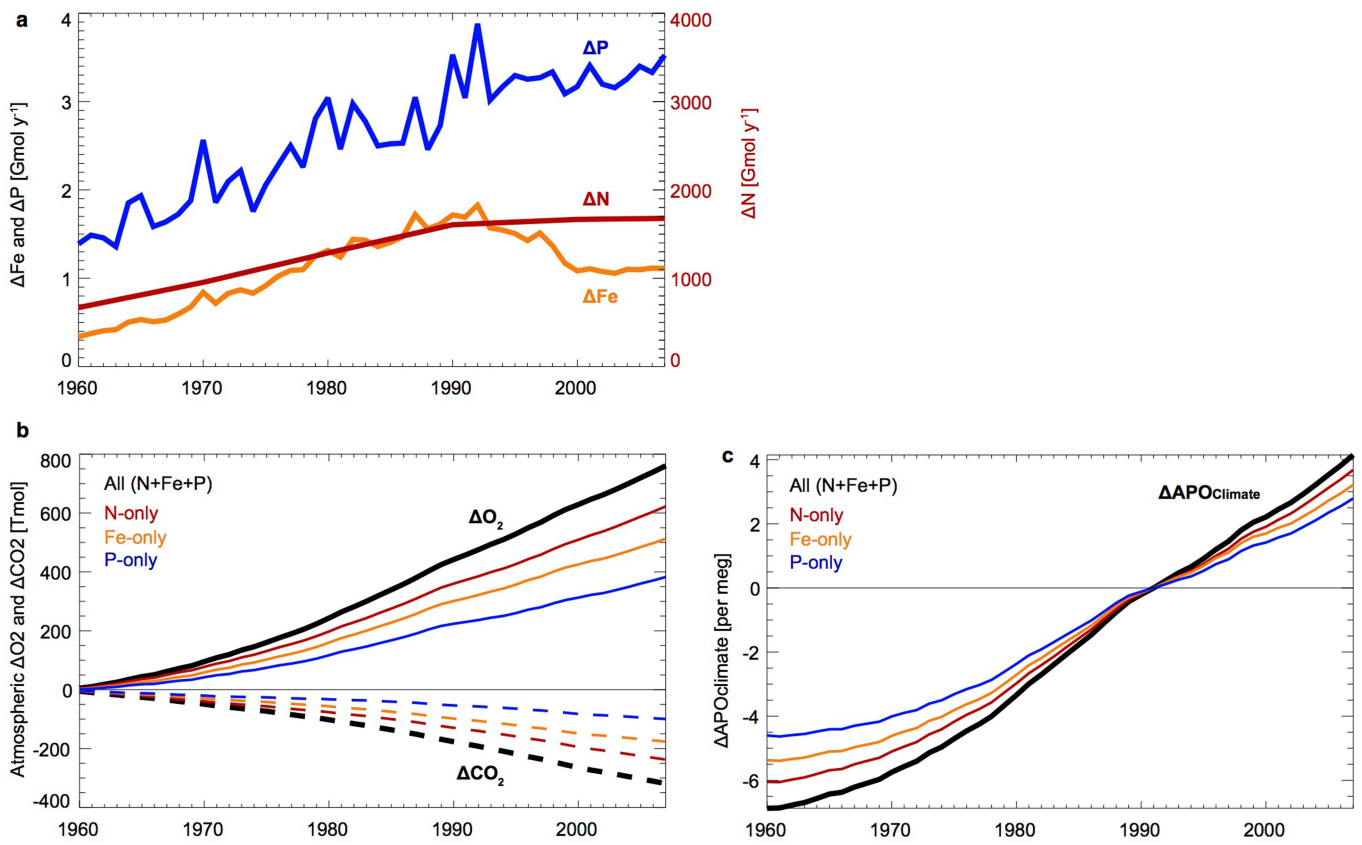
Extended Data Fig. 1 | Effects of anthropogenic aerosols on APO.
a, Anomaly, relative to 1850 levels, in deposition of atmospheric anthropogenic aerosols (N, P and Fe) at the air–sea interface between 1960 and 2007, derived from model simulations with and without aerosols[22].

b, Impact of aerosol eutrophication on atmospheric O_2 (solid lines) and CO_2 (dashed lines) for all aerosols (black lines) and for each aerosol taken individually (coloured lines). **c**, Overall impact of aerosol eutrophication on $\Delta APO_{Climate}$ referenced to the first year that has observations (1991).
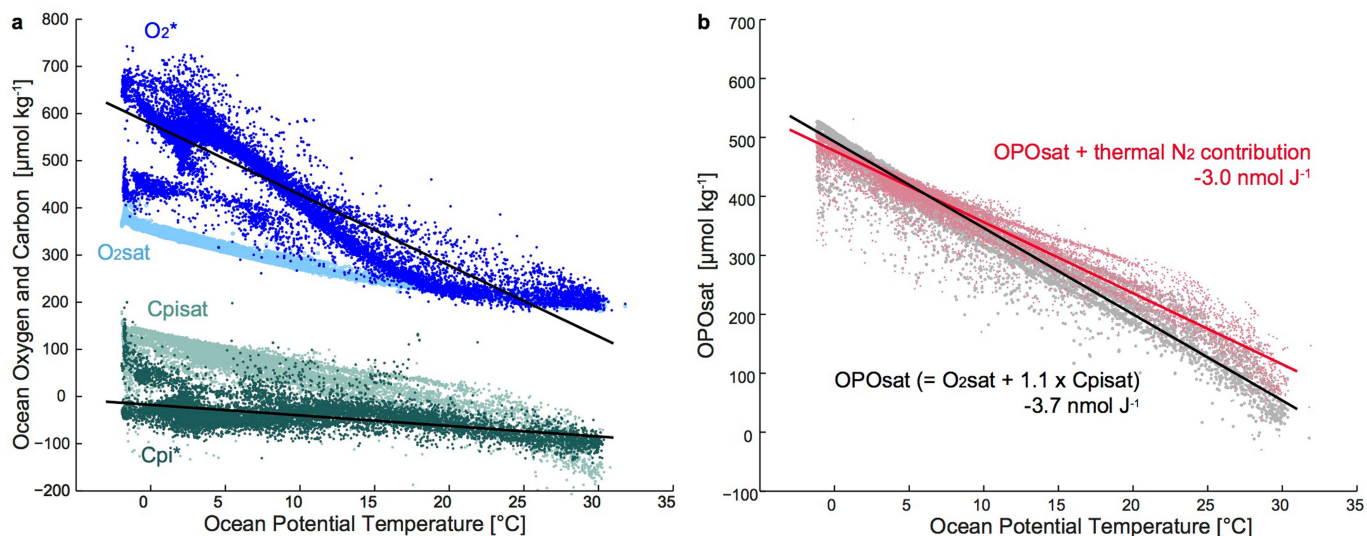
Extended Data Fig. 2 | Solubility-driven changes in ocean oxygen and carbon concentrations. a, Ocean observations of O_2^*, O_{2sat}, C_{pi}^* and C_{pisat} as a function of potential temperature in the Glodapv2 database[32]. **b**, OPO_{sat} ($= O_{2sat} + 1.1 C_{pisat}$, in grey) and the expected effects on APO owing to the combined effects of OPO_{sat} and the thermal exchanges of N_2 ($= O_{2sat} + 1.1 C_{pisat} - X_{O2} / X_{N2} [N_2 - mean(N_2)]$, in red). For clarity only 16×10^3 points randomly picked out of the 78,456 data points available

are shown for each variable. Note that very low values of O_2^* (around 450 μmol kg^{-1}) at low temperature (less than 10 °C) correspond to data collected in the Arctic Ocean, where phosphate concentrations (used for O_2^* calculation) are comparatively lower than in other cold ocean regions. Low O_2^* values in the Arctic explain the relatively low values of OPO shown in Extended Data Fig. 3a at temperatures below 10 °C.
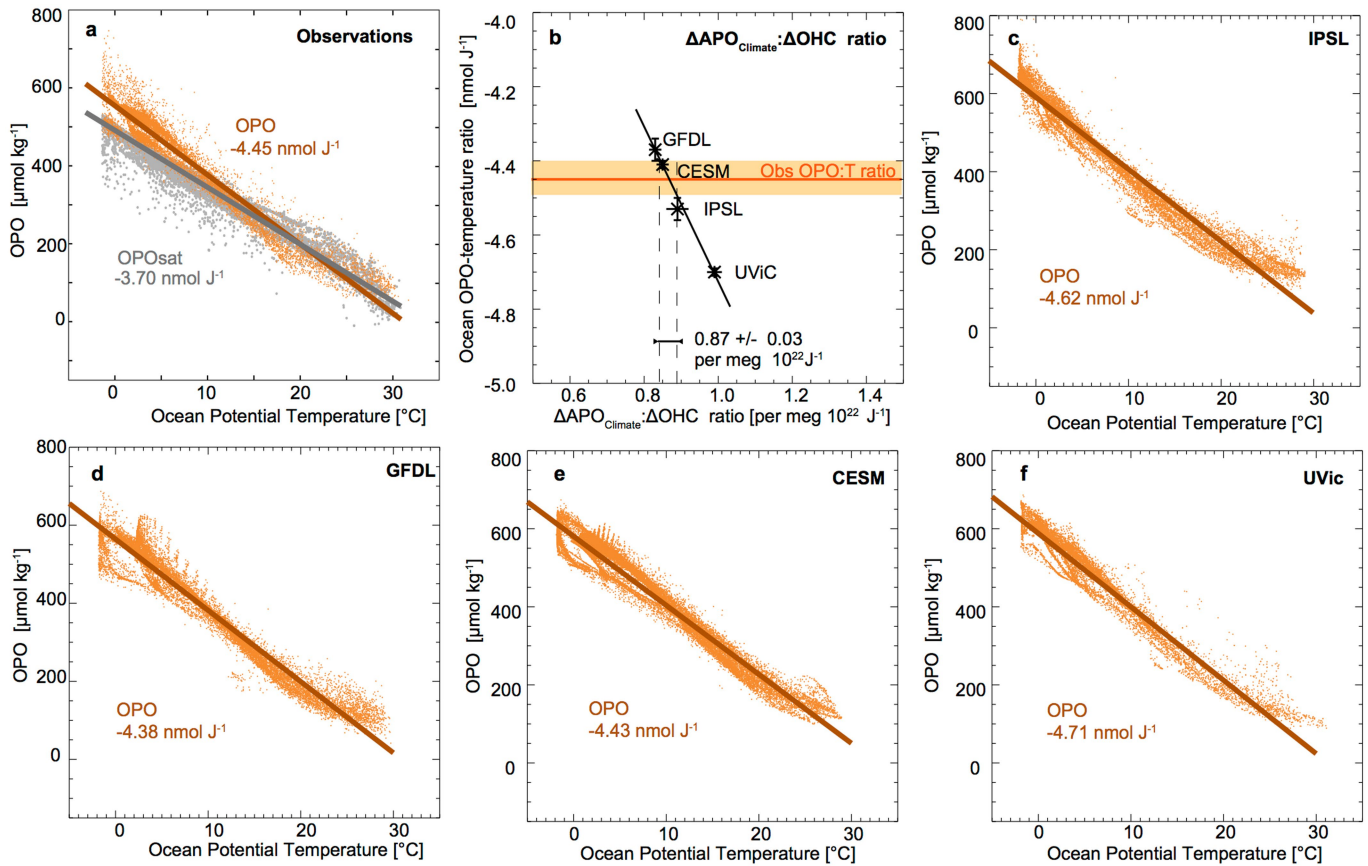
Extended Data Fig. 3 | Link between OPO, APO$_{Climate}$ and ocean heat.
a, **c–f**, OPO concentrations (yellow) and OPO concentrations at saturation based on O_2 and CO_2 solubility (OPO$_{sat}$, grey) as a function of ocean temperature in the GLODAPv2 database[32] (**a**) and four Earth-system models (IPSL, GFDL, CESM and UViC; **c–f**). Slopes give the OPO-to-temperature ratios in nmol J^{-1}. **b**, The link between $\triangle$APO$_{Climate}$ and changes in ocean heat content (that is, $\triangle$APO$_{Climate}$-to-$\triangle$OHC ratio) in the four models is tied to their OPO-to-temperature ratios and can be constrained using the observed OPO-to-temperature of 4.45 nmol J^{-1} (vertical dashed lines). To avoid visual saturation, only 16,000 points, picked randomly, are shown for OPO.
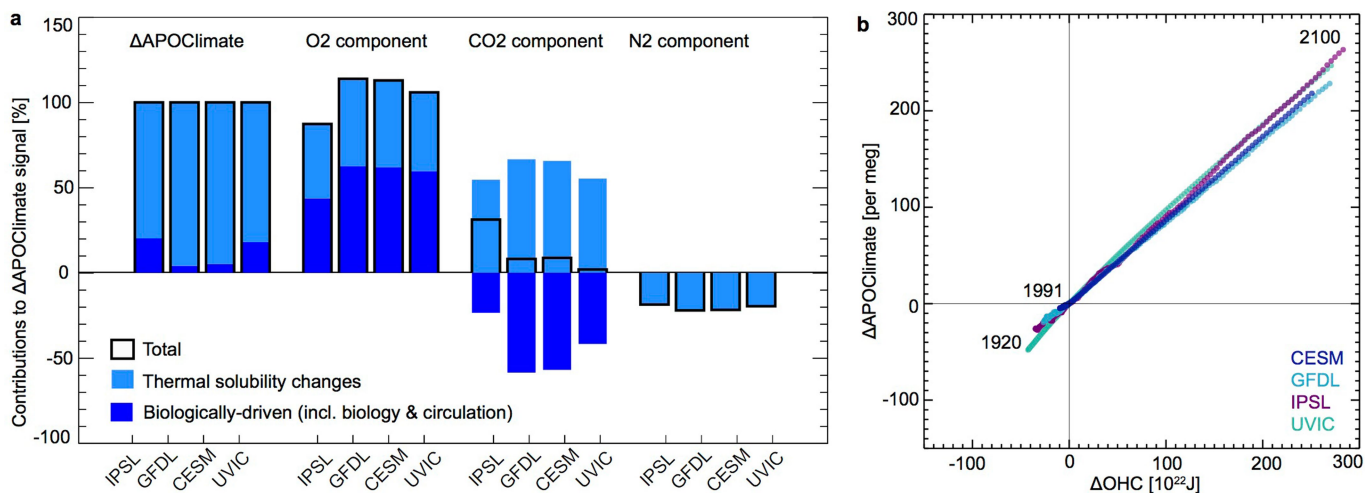
Extended Data Fig. 4 | Changes in APO$_{Climate}$ (ΔAPO$_{Climate}$) and ocean heat content (ΔOHC) in four Earth-system models. a, Simulated ΔAPO$_{Climate}$ (black outlines) are decomposed into the contributions (percentage of total) from changes in ocean thermal saturation (light blue) and biologically driven changes (dark blue), the latter including changes in photosynthesis/respiration and changes in ocean circulation that transport and mix gradients of biological origin. For each model, ΔAPO$_{Climate}$ is further decomposed into its O$_2$, CO$_2$ and N$_2$ components—that is, how much of ΔAPO$_{Climate}$ is explained by changes in O$_2$, CO$_2$ and N$_2$ air–sea fluxes due to ocean saturation changes and biologically driven changes. **b**, Model ΔAPO$_{Climate}$-to-ΔOHC ratios over the 180 years of simulation (referenced to year 1991) in per meg per 10^{22} J units are: 0.85 ± 0.01 (CESM), 0.83 ± 0.01 (GFDL), 0.89 ± 0.03 (IPSL) and 0.99 ± 0.02 (UVic).

Extended Data Table 1 | Sources of the hydrographic databased estimates of global changes in ocean heat content (△OHC) used in Fig. 1

Label in Fig 1	0 to 2000 m depth range	2000 to 6000 m depth range
PMEL	Ref. 10	Ref. 11
MRI	Ref. 9	Ref. 11
NCEI	Update of Ref. 31	Ref. 11
CHEN	Ref. 12	Ref. 11

The estimates are taken from refs 9–12.

Extended Data Table 2 | Linear trends in global ocean heat content

	1991-2016 ΔOHC trend (±1-σ)	1993-2016 ΔOHC trend (±1-σ)	2007-2016 ΔOHC trend (±1-σ)
APO$_{Climate}$	1.33 ± 0.20	-	-
PMEL	-	1.35 ± 0.10	1.16 ± 0.20
MRI	1.00 ± 0.11	1.03 ± 0.12	1.23 ± 0.22
NCEI	0.89 ± 0.08	0.90 ± 0.09	1.28 ± 0.16
CHEN	1.07 ± 0.07	1.10 ± 0.08	1.09 ± 0.10

Units are 10^{22} J yr^{-1}. Trends and $\pm1\sigma$ uncertainty ranges are given for hydrographic (in situ temperature) and atmospheric (APO) data over the depth range 0–6,000 m. See Extended Data Table 1 for literature sources of estimates.

Extended Data Table 3 | Contributions to $\triangle APO_{OBS}$, $\triangle APO_{FF}$ and $\triangle APO_{Cant}$ and associated uncertainties ($\pm 1\sigma$) during the observation period 1991–2016

	Mean value	References	1-σ uncertainty	References
			$\triangle APO_{OBS}$	
Corrosion			± 0.3 per meg yr^{-1}	
Leakage			± 0.2 per meg yr^{-1}	
Desorption			± 0.1 per meg yr^{-1}	
Thermal fractionation			± 2 per meg (± 4 before July 1992)	Ref. 36
Scale systematic error			2% on $\delta(O_2/N_2)$ contribution	
			$\triangle APO_{FF}$	
			Oxidative Ratios R_i	
Coal	1.17		± 0.03	
Oil	1.44	Ref. 36	± 0.03	Ref. 36
Gas	1.95		± 0.04	
Cement	0.0		± 0.00	
Flaring	1.98		± 0.07	
			Emissions $\triangle CO2_i$	
Coal			$\pm 7.0\%$	
Oil	Time varying	Ref. 20	$\pm 5.5\%$	Ref. 35
Gas			$\pm 6.5\%$	
Cement			$\pm 12\%$	
Flaring			$\pm 12\%$	
			$\triangle APO_{Cant}$	
$\triangle Cant_0$	Time varying (~2 to 3 PgC yr^{-1})	Ref. 21	1-σ of 10 experiments (<0.3 PgC yr^{-1})	Ref. 21
			+ 1% uncertainty (<0.03 PgC yr^{-1}) (atmospheric CO_2 history)	this study
$\triangle Cant'$	0.05 PgC yr^{-1} (0.12 per meg yr^{-1})	this study	± 0.05 PgC yr^{-1} (± 0.12 per meg yr^{-1})	this study

The estimates are taken from refs 20,21,35,36.

Extended Data Table 4 | Temporal evolution of the cumulative contributions to global APO changes and their 1σ uncertainties

year	$\Delta APO_{Climate}$	1-σ	ΔAPO_{OBS}	1-σ	ΔAPO_{FF}	1-σ	ΔAPO_{Cant}	1-σ	ΔAPO_{AtmD}	1-σ
1991	0.00	0.00	0.00	0.00	0.00	0.00	0.00	0.00	0.00	0.00
1992	1.50	4.00	-6.80	4.00	-4.00	0.30	-4.90	0.10	0.50	0.30
1993	3.90	4.10	-12.90	4.00	-8.00	0.40	-9.70	0.30	0.80	0.40
1994	3.50	2.30	-22.30	2.20	-12.10	0.50	-14.80	0.40	1.10	0.50
1995	6.50	2.50	-28.40	2.30	-16.20	0.60	-20.10	0.50	1.30	0.70
1996	5.40	2.70	-39.00	2.50	-20.40	0.70	-25.50	0.70	1.60	0.80
1997	7.50	3.00	-46.10	2.70	-24.70	0.80	-30.80	0.90	1.90	0.90
1998	11.30	3.40	-52.40	2.90	-29.00	0.90	-36.80	1.10	2.10	1.10
1999	14.90	3.70	-58.70	3.20	-33.40	1.10	-42.60	1.20	2.40	1.20
2000	10.00	4.20	-73.40	3.60	-37.90	1.20	-48.20	1.40	2.70	1.30
2001	9.60	4.50	-83.90	3.90	-42.50	1.30	-54.00	1.60	2.90	1.50
2002	15.70	4.80	-87.90	4.10	-47.10	1.40	-59.80	1.70	3.20	1.60
2003	14.00	5.40	-100.40	4.50	-51.80	1.60	-66.10	1.90	3.50	1.70
2004	15.10	5.80	-110.20	4.90	-56.70	1.70	-72.40	2.00	3.70	1.90
2005	18.40	6.30	-117.80	5.20	-61.70	1.80	-78.60	2.30	4.00	2.00
2006	19.60	6.70	-127.90	5.60	-66.80	2.00	-85.10	2.40	4.30	2.10
2007	16.60	7.30	-142.10	6.10	-71.90	2.20	-91.60	2.60	4.50	2.30
2008	16.30	7.80	-153.90	6.50	-77.10	2.40	-98.10	2.90	4.80	2.40
2009	19.40	8.20	-162.00	6.80	-82.20	2.60	-104.50	3.00	5.10	2.50
2010	19.10	8.80	-174.30	7.20	-87.40	2.80	-111.50	3.20	5.40	2.70
2011	19.70	9.30	-185.40	7.60	-92.70	3.00	-118.30	3.40	5.60	2.80
2012	20.90	9.80	-196.20	8.10	-98.10	3.20	-125.10	3.50	5.90	3.00
2013	18.80	10.50	-210.30	8.60	-103.40	3.40	-132.10	3.80	6.20	3.10
2014	22.90	11.00	-218.70	9.00	-108.70	3.60	-139.50	3.90	6.50	3.20
2015	22.90	11.50	-231.10	9.50	-114.20	3.80	-146.70	4.20	6.70	3.40
2016	23.20	12.20	-243.70	10.10	-119.70	4.00	-154.30	4.20	7.00	3.50

Units are per meg.

Extended Data Table 5 | Trends in air–sea flux of O$_2$, CO$_2$ and APO due to anthropogenic aerosol deposition

Trends 1980 to 2007	N-only	Fe-only	P-only	All (N+Fe+P)
O$_2$ [Tmol y^{-1}]	15.5	12.9	9.6	19.0
CO$_2$ [Tmol y^{-1}]	-6.1	-4.6	-2.6	-8.3
APO$_{AtmD(O2)}$ [per meg y^{-1}]	0.42	0.35	0.26	0.51
APO$_{AtmD(CO2)}$ [per meg y^{-1}]	-0.18	-0.14	-0.08	-0.24
APO$_{AtmD}$ [per meg y^{-1}]	0.24	0.21	0.18	**0.27**

Trends in APO due to atmospheric deposition (ΔAPO$_{AtmD}$) are decomposed into contributions from the O$_2$ flux only (APO$_{AtmD(O2)}$) and the CO$_2$ flux only (APO$_{AtmD(CO2)}$). Results are from model simulations[22]. Anomalies in air–sea flux are positive towards the atmosphere. The total trend used in this study is in bold type.